RSC Advances

ROYAL SOCIETY OF CHEMISTRY

www.rsc.org/advances

RSC Advances

RSCPublishing

COMMUNICATION

Branching and size of CTAB-coated gold nanostars control the colorimetric detection of bacteria

Cite this: DOI: 10.1039/xoxxoooooox

Mohit S. Verma[a,b,+], Paul Z. Chen[a,+], Lyndon Jones[a,c], and Frank X. Gu[a,b,*]

Received ooth January 2012,
Accepted ooth January 2012

DOI: 10.1039/xoxxoooooox

www.rsc.org/

Rapid detection of pathogenic bacteria is challenging because conventional methods require long incubation times. Nanoparticles have the potential to detect pathogens before they can cause an infection. Gold nanostars have recently been used for colorimetric biosensors but they typically require surface modification with antibodies or aptamers for cellular detection. Here, CTAB-coated gold nanostars have been used to rapidly (<5 min) detect infective doses of a model gram-positive pathogen *Staphylococcus aureus* by an instrument-free colorimetric method. Varying the amounts of gold nanoseed precursor and surfactant can tune the size and degree of branching of gold nanostars as studied here by transmission electron microscopy. The size and morphology of gold nanostars determine the degree and rate of color change in the presence of *S. aureus*. The optimal formulation achieved maximum color contrast in the presence of *S. aureus* and produced a selective response in comparison to polystyrene microparticles and liposomes. These gold nanostars were characterized using UV-Visible spectroscopy to monitor changes in their surface plasmon resonance peaks. The visual color change was also quantified over time by measuring the RGB components of the pixels in the digital images of gold nanostar solutions. CTAB-coated gold nanostars serve as a promising material for simple and rapid detection of pathogens.

1. Introduction

Gold nanostars are an interesting class of materials because of their excellent performance in colorimetric biosensors,[1-4] surface enhanced Raman spectroscopy (SERS),[5-11] imaging and therapy,[12, 13] as well as recently in solar cell power conversion.[14] The optical and electrical characteristics of gold nanostars are governed by their size and degree of branching.[11, 15] Hence, control over these parameters is essential and has previously been demonstrated using methods such as seed-free growth,[16] the use of poly(vinylpyrrolidine) (PVP),[11, 17, 18] and even surfactant-free synthesis, but a systematic study of seed-mediated synthesis assisted by the surfactant, cetyltrimethylammonium bromide (CTAB) is lacking. The use of nanoseed precursor and surfactant offers the opportunity to control the size and degree of branching of the nanostars using these two simple parameters. The morphology of nanostars determines the peak of light absorption and hence the color of gold nanostars. The peak of absorption in gold nanoparticles changes with their aggregation state. The shift in this peak causes a drastic color change that is detectable by the naked eye and is ideal for application in a biosensor. Furthermore, nanoparticles have increased kinetics in solution when compared with their microparticle counterparts, suggesting that rapid detection may be feasible using a biosensor platform at the nano-scale.[19, 20]

Food poisoning continues to cause severe illness around the world and leads to hospitalization of unsuspecting patients. The concentration of pathogens necessary for successfully infecting the host is known as the infective dose. Simple and rapid detection of foodborne pathogens at their infective dose is a key step in preventing the spread of contamination.[21] Conventional methods for the detection of food-borne pathogens include culture counting, immunology and polymerase chain reaction, but these methods suffer from the drawbacks of long incubation time, interference from contaminants and the requirement of specialized equipment, respectively.[22]

These shortcomings have inspired the advancement of biosensors that utilize optical, electrochemical and mass-based transduction. Typically, these biosensors involve the use of specialized equipment such as a spectrophotometer, electrochemical cell or quartz crystal microbalance and hence cannot be easily implemented outside the laboratory.[20, 22-24] Thus, there exists a need for a simple and rapid method of pathogen detection that does not require specialized training or expensive equipment.[25] We chose *Staphylococcus aureus*, a gram-positive micro-organism, as a model pathogen for testing the detection capabilities of our gold nanostars. *S. aureus* often causes food poisoning by producing enterotoxins which induce symptoms of sudden vomiting, diarrhea, nausea, malaise, abdominal cramps and pain. Since the main mechanism of infection for *S. aureus* involves secreted toxins that need to diffuse out of the bacterium, it

is considered a distant action pathogen. Such pathogens require a high concentration (10^5 to 10^6 CFU/mL for *S. aureus*) in the inoculum to successfully infect the host.[26]

We expect that aggregation of gold nanostars can be induced by the presence of *S. aureus* via electrostatic interactions between the positively charged CTAB-coated gold nanostars and negatively charged cell walls of *S. aureus.* Such aggregation will lead to a rapid and drastic color change. This principle has been demonstrated in the literature when gold nanoparticles were modified by either antibodies[4] or aptamers[27] specific to the pathogen of interest. While recent detection method of *S. aureus* claims to be rapid, it still requires 1.5 hours, complex modification of gold nanoparticles as well as specialized equipment.[27] The control of the assembly/disassembly of unmodified gold nanoparticles has led to detection of small molecules, metal ions, DNA and proteins but not whole cells. Studies suggest that cationic gold nanoparticles might aggregate around bacteria[28, 29] but the effect of size and morphology of gold nanostars on the aggregation kinetics has not been explored before. Here, we demonstrate for the first time that CTAB-coated gold nanostars can be used for rapid (<5 min) instrument-free colorimetric detection of pathogens in solution. We hypothesize that the degree and rate of color change of gold nanostars in the presence of *S. aureus* will be defined by the degree of branching and the particle size.

2. Experimental

2.1. Materials

Gold (III) chloride hydrate ($HAuCl_4 \cdot xH2O$), Hexadecyltrimethylammonium bromide (CTAB), sodium borohydride, silver nitrate, and L-ascorbic acid were purchased from Sigma-Aldrich (Oakville, ON, Canada). Trisodium citrate dihydrate was purchased from Thermo Fisher Scientific (Burlington, ON, Canada). All materials were used without further purification. Transparent 96-well microplates, BD trypticase soy agar (TSA) culture plates, BD nutrient broth, sodium chloride (ACS grade), Nalgene sterilization filter units and calcium alginate swabs were purchase from VWR (Mississauga, ON, Canada). Polybead® Carboxylate Microspheres 3.00 µm, 1.00 µm and 0.10 µm were purchased from Polysciences, Inc. (Warrington, PA, USA) and used as model negatively charged polystyrene microparticles. 1,2-dimyristoyl-sn-glycero-3-phosphocholine (DMPC), 1,2-dimyristoyl-*sn*-glycero-3-phospho-(1'-rac-glycerol) (DMPG) and 1,2-dimyristoyl-*sn*-glycero-3-phosphoethanolamine (DMPE) phospholipids were purchased from Avanti Polar Lipids, Inc. (Alabaster, AL, USA). 400 mesh formvar/carbon coated copper grids were obtained from Canemco Inc (Gore, QC, Canada). *S. aureus* (ATCC 6538) was provided by Dr. David McCanna from Dr. Lyndon Jones' lab at the University of Waterloo. The vials used for gold nanostar synthesis were rinsed with Millipore water before use.

2.2. Synthesis of gold nanoseed precursor

The gold nanoseed precursor was synthesized using a modified version of a previously described simple two-step one pot process.[13] First, a gold (III) chloride hydrate and trisodium citrate dihydrate solution was prepared with final concentrations of 2.5×10^{-4} M and 10^{-4} M, respectively, in 20 mL of Millipore water. Then, under moderate stirring freshly prepared, ice-cold sodium borohydride (0.1 M, 60 µL) was quickly added. Immediately, the solution turned brown-pink and slowly developed into its final red color. The sample was stored overnight in the dark in ambient conditions. The solution was then filtered (0.2 µm) and stored at 4 °C until use. Gold nanoseed solutions were found to be stable for weeks at this temperature. Uniform spherical gold nanoparticles approximately 4-5 nm in diameter were produced.

2.3. Synthesis of CTAB-coated gold nanostars

Gold nanostar samples were synthesized using CTAB as a negative template using a modified procedure.[13] The amount of CTAB and gold (III) chloride hydrate were varied to yield the entire nanostar set (n = 30) with varying sizes and morphologies. CTAB (7.33 mM; 125 mg CTAB in 46.88 mL Millipore water) was dissolved by probe sonication (2 seconds on, 1 second off; 25% amplitude) for 20 minutes. This concentration was designated as 125 mg CTAB, based on the initial dissolved amount, for ease of naming convention. After this, the 125 mg CTAB solution was diluted with Millipore water 1:5 (1.466 mM, designated 25 mg CTAB), 2:5 (2.932 mM, designated 50 mg CTAB), 3:5 (4.398 mM, designated 75 mg CTAB), and 4:5 (5.864 mM, designated 100 mg CTAB) for 30 total samples (15 mL, 6 per CTAB concentration). Gold (III) chloride hydrate (0.64 mL, 11 mM) and silver nitrate (0.096 mL, 0.01 M) were added to the CTAB solution under vigorous stirring for 1 minute. Then, L-ascorbic acid (0.103 mL, 0.1 M) was added dropwise. Upon addition of the last drop of L-ascorbic acid, the solution turned clear, and the appropriate volume of gold nanoseed was immediately added. For each CTAB concentration 400, 320, 240, 160, 80, or 32 µL of gold nanoseed was added for 15 mL of initial CTAB solution, resulting in a final 5 x 6 set. After seed addition, each sample was allowed to stir for another 1.5 minutes. The samples were left in the dark in ambient conditions until use. Gold nanostars were found to be stable in the dark at room temperature for months.

2.4. Characterization of gold nanostars

The gold nanostars were characterized using transmission electron microscopy (TEM) for sizing and UV-Visible (UV-Vis) spectrophotometry for absorbance spectra. TEM and UV-Vis spectrophotometry were performed using a Philips CM10 and BioTek Epoch Microplate Spectrophotometer, respectively. TEM samples were prepared by drying 5 µL of the samples described above overnight on formvar/carbon coated copper grids. UV-Vis absorbance spectroscopy was performed in duplicates for 300 µL samples in a 96-well plate. Zeta potential was measured using Malvern Zetasizer and gold nanostars as well as bacteria were suspended in 0.85% saline (with ~0.006% broth) to mimic the testing conditions.

TEM images (92,000x) of the all gold nanostars were sized manually with National Institute of Health ImageJ software (n

= 10 each). Calibrated by the scale bars, nanostars were profiled, and five particularities were measured for each nanostar: branch length (Fig. 1 a), branch width (Fig. 1 b), total diameter (Fig. 1 c), minor diameter (Fig. S1), and number of branches (Fig. 1 d and Fig. S2 for average number and distribution, respectively). Total diameter was defined as the longest total length of a nanostar given that the length passes through its geometric center. Conversely, minor diameter was defined as the shortest length through the geometric center. A branch was defined as an extrusion from the expected curvature of a nanostar given that the branch width is less than or equal to half the core diameter. Branch length and width were defined as the measurement from the expected curvature of the nanostar to the branch tip and the perpendicular width at half the branch length, respectively (Scheme 1).

2.5. *Staphylococcus aureus* culture

S. aureus was cultured on TSA plates by using alginate swabs and incubating the plates at room temperature for two nights. A 2.55% saline solution was prepared and sterilized by using Nalgene filters and ~0.006% of nutrient broth was added to the saline to preserve *S. aureus* during tests. *S. aureus* was transferred to saline solution by adding 5 mL of saline (with ~0.006% broth) to the TSA plate and using alginate swabs to dislodge the bacteria from the plates. *S. aureus* was washed with saline (with ~0.006% broth) solution seven times by centrifugation at 4,000 rpm for 10 minutes. The stock solution of *S. aureus* was diluted 100 times in saline (with ~0.006% broth) and used for testing with gold nanostars. The concentration of *S. aureus* was determined by direct plate counts method.

2.6. Colorimetric detection of *Staphylococcus aureus* using various gold nanostars

All 30 of the gold nanostars synthesized were tested to characterize their potential as an instrument-free colorimetric detection platform. 200 µL of each nanostar solution was input into a 96-well microplate placed on top of an x-ray film viewer for homogenous white light illumination. The nanostars were arranged such that columns corresponded increasing (25 to 125 mg from left to right) CTAB amount, while rows corresponded to decreasing (400 to 32 µL from top to bottom) seed volume. The nanostars were then imaged using a Canon EOS Rebel T3 with constant settings. Subsequently, 100 µL of $5x10^5$ CFU/well *S. aureus* was added to each well at time = 0. The color change was then imaged for 2 hours using intervals of about 25 seconds. The image for each subsequent time point was normalized by subtracting the initial image without *S. aureus* using MathWorks MATLAB®. The red, green, blue (RGB) values of the subtracted images were extracted from 200 pixels per well. These values were averaged for each time point and plotted against time for obtaining Fig. 3 c. These images were also arranged as chronological frames for use as a continuous video (Supplementary Video 1). After determining the optimal formulation of gold nanostars, the effect of purification and excess CTAB concentration on bacteria detection was evaluated. The gold nanostars were centrifuged at 10000 rpm for 15 minutes. The supernatant was discarded and the precipitate was resuspended in either Millipore water (0 mg CTAB) or solutions with CTAB concentrations matching those used during synthesis (25, 50, 75, 100, 125 mg). Next, 100 µL of saline (with ~0.006% broth) or *S. aureus* with a normalized absorbance of 0.1 at 660 nm was added to 200 µL of each of the gold nanostar solutions and incubated overnight. Photographs were then obtained using the digital camera.

2.7. Comparison of *Staphylococcus aureus* to charged particles

In order to demonstrate selectivity, a solution of *S. aureus* was prepared in saline (with ~0.006% broth) to obtain normalized absorbance of 0.1 at 660 nm and this results in a concentration of approximately $8x10^6$ CFU/well as determined by plate counts method. Since bacteria and particles cannot be exactly at the same concentration, they were compared by preparing the solutions at the same normalized absorbance of 0.1 at 660 nm. Polystyrene particles were diluted in saline (with ~0.006% broth). Liposomes were prepared according to manufacturer's recommendation. DMPC was dissolved in chloroform at a concentration of 10 mg/mL, while DMPG and DMPE were dissolved in a mixture of chloroform:methanol:water (65:35:8 v/v/v) at a concentration of 10 mg/mL. The phospholipid solutions were first dried under nitrogen and then *in vacuo* overnight. Saline (with ~0.006% broth) was added to the vials containing DMPC and DMPG at 30 °C, and DMPE at 60 °C. The phospholipids were allowed to rehydrate for several hours at the respective elevated temperatures. Size reduction was performed by sonicating each of the samples using a Branson probe sonicator for 10 minutes at 25% amplitude and 1 second on, 0.5 second off pulses. Each of the solutions were diluted in saline (with ~0.006% broth) to obtain the appropriate absorption. 100 µL of the particle solutions were then added to the 200 µL of optimal gold nanostar solution in a 96-well microplate. The solutions were incubated overnight and UV-Vis absorption spectra were obtained.

3. Results and Discussion

3.1. Synthesis of gold nanostars and morphology characterization

Gold nanostars were synthesized at room temperature via a seed-mediated growth mechanism using cetyltrimethylammonium bromide (CTAB) surfactant as a template.[13] The mechanism of anisotropic growth in gold nanoparticles is currently being investigated and often the growth of gold nanostars is compared to that of gold nanorods, because both morphologies use CTAB surfactant as a negative template and silver ions for creating active sites.[30-34] In the case of nanostars, the twin defects on the surface of the seed are postulated to weaken the binding of the positively charged CTAB surfactant, which allows the growth of branches at these sites.[32] Also, silver can be deposited on the surface of the seed by underpotential[31] and produce additional defects, which in turn act as active sites for growth of branches.[32, 33, 35] We hypothesize that the

surface morphology and particle size of gold nanostars can be controlled by changing the amount of gold seed precursor (32, 80, 160, 240, 320 or 400 µL) and CTAB (25, 50, 75, 100, 125 mg) added to the formulation. To test this hypothesis, we synthesized 30 types of gold nanostars by using all possible combinations of these two parameters, while keeping the amount of silver nitrate, L-ascorbic acid and gold salt in solution constant. These nanostars were characterized using transmission electron microscopy (TEM) to determine their size and surface morphology and using UV-Vis spectroscopy to determine their absorption spectra. We then demonstrated that the gold nanostars change color drastically in the presence of *S. aureus* as compared to a saline (with ~0.006% broth) control.

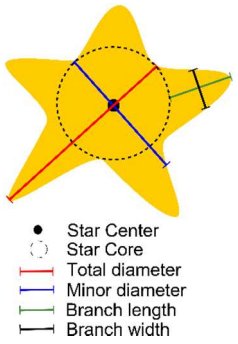

Scheme 1 Definition of various parameters for characterizing a gold nanostar. Total diameter is the maximum length of line segment that passes through the center of the star; Minor diameter is the minimum length of the line segment that passes through the center of the star; branch length is the distance from the tip of the branch to the expected curvature of the star core; branch width is the width measured at half the branch length.

The TEM images of the 30 samples of gold nanostars show that the total size of nanostars is mostly controlled by the amount of gold nanoseed added, while the degree of branching and branch length are controlled by the CTAB amounts (Fig. 1). Increasing the amount of seed decreases the total size because more growth sites are present and the total amount of gold available for growth in solution is kept constant. Increasing the amount of CTAB increases the branch length and the average number of branches because the number of CTAB micelles per seed increases. We quantified the size and degree of branching for each of the 30 samples by measuring the total diameter, minor diameter, branch length and branch width, as defined in Scheme 1. The total diameter (Fig. 1 c) and minor diameter (Fig. S1) showed similar dependence on seed and CTAB concentration, as diametric and branch growth occurs simultaneously when gold is available in solution. This also leads to the relatively uniform growth of branch width under the same conditions as growth of the stars (Fig. 1 b). The total diameter ranged from 31 nm to 113 nm for 400 µL and 32 µL seed sets respectively, while the length of branches ranged from 3 nm to 17 nm for 25 mg CTAB and 125 mg CTAB sets respectively (Fig. 1 a, c). The changes in surfactant and seed not only affect the dimensions of the branches but also the average number of branches, which ranges from one to six (Fig. 1 d). We believe this is because the higher concentration of CTAB per seed allows better adsorption of CTAB, which in turn promotes anisotropic growth at multiple sites. Additionally, the distribution of stars with increasing number of branches also varies with the amount of seed and CTAB. Low seed volumes and high concentration of CTAB are necessary for a higher fraction of highly branched nanostars (Fig. S2). Although there are some rare outliers in the TEM images of single nanostars due to the nature of selecting individual nanoparticles, the trends of size and branching are clearly visible in the images as well as the plots that follow in Fig. 1.

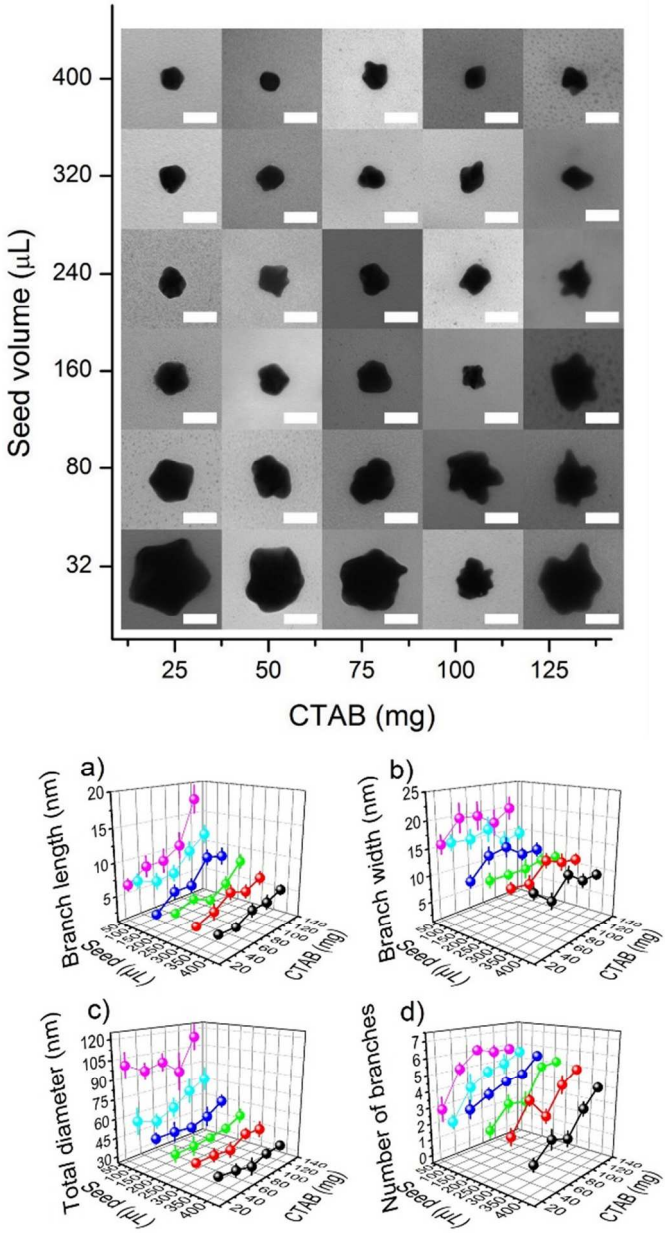

Fig. 1. Top: Transmission electron microscopy (TEM) images of thirty nanostar samples (scale bar: 50 nm). Bottom: Various parameters defined in Scheme 1, measured from the TEM images for nanostars: a) Branch length (n = 10; mean ± S.E) b) Branch width (n = 10; mean ± S.E), c) Total diameter (n = 10; mean ± S.D.), d) Number of branches (n = 10; mean ± S.E.)

3.2. Colorimetric characterization of gold nanostars

The color of gold nanoparticles is determined by the size of the particles because of their surface plasmon resonance. A change in the surface plasmon resonance of the particles can be characterized by the absorption peak of UV-Vis spectroscopy.[32, 34-36] As seen in Fig. 2 a), varying size and the degree of branching yields nanostars with different solution colors. The lowest CTAB, highest seed sample yields a red color. This sample lacks significant branching and thus is found to have a more spherical morphology, as we previously described. Spherical gold nanoparticles have been extensively studied in the past, and as we observed, give the solution a distinct red color.[37]

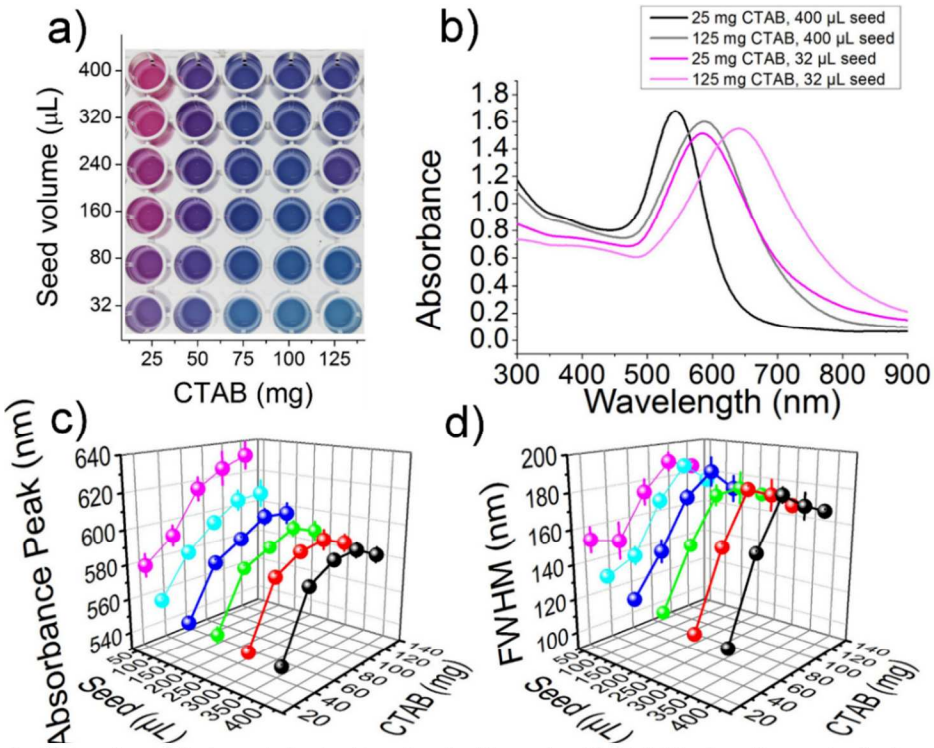

Fig. 2. Optical properties of gold nanostars: a) Photograph showing the color of gold nanostars b) UV-Visible absorption spectra for four of the gold nanostars with varying seed and CTAB concentrations. Effect of CTAB and seed concentrations on c) UV-Visible absorbance peaks (n = 6, mean ± S.D.), and on d) Full Width Half Maximum (FWHM) (n = 6, mean ± S.D.)

Decreasing seed and increasing CTAB causes the gold nanostar solutions to be violet and then blue, resulting from a shift in plasmon resonances caused by increased degree of branching and general star-like morphology.[13, 38] The dependence of absorption peak and width on the degree of branching has rarely been explored.[12] We repeated the synthesis of the 30 stars three times and measured the absorption spectra from 300 nm to 900 nm with a step size of 1 nm. As an example, we plotted the complete spectra of the four extreme synthesis data points (Fig. 2 b). We also extracted the peaks and full width half maximum values (FWHM) from the spectra of all the nanostars (Fig. 2 c,d). Increasing size of the nanostars by decreasing seed leads to a red shift in the absorption peak and also broadens the width. Additionally, there is a significant jump in the peak and FWHM when increasing the CTAB from 25 to 50 mg even though the size of the particles only varies slightly. This jump suggests that a minimum concentration of CTAB is necessary for changing the morphology of nanoparticles from spheres to stars and causing a shift in absorbance peak of about 60 nm.[13] Interestingly, a characteristic drop in the peak position and FWHM occurs at the highest CTAB concentration for all seed volumes when the number and length of branches is the highest. This drop is in agreement with previously modeled data, where a slight blue shift in absorbance peak is observed when the number of branches was increased from four to ten.[12] The drop in the FWHM at highest CTAB concentration also suggests that the size distribution of nanostars is narrower.[12] This is most likely because a higher concentration of CTAB allows for more homogenous adsorption of CTAB on the seeds, thereby synthesizing more monodisperse gold nanostars.

3.3. Colorimetric detection of *Staphylococcus aureus*

Next, we tested the ability of each of the gold nanostars to detect gram-positive bacteria *S. aureus* by adding them to gold nanostars in 96-well microplates. *S. aureus* was suspended in 2.55% saline solution (with ~0.006% broth) and thus this saline was used as a negative control. Fig. 3 a) shows that the stars synthesized with the lowest seed amounts turn clear in saline (with ~0.006% broth) solution. This color change can be explained by the colloidal instability of larger gold nanostars. In contrast, nanostars synthesized with higher seed values are more stable and only change color in the presence of *S. aureus*. While qualitative color change is intense and can be easily observed using the naked eye, quantification of the color was

achieved by measuring the red, green and blue (RGB) components of each sample. We collected several images over two hours at an interval of about 25 seconds while leaving the samples undisturbed and then normalized each image with *S. aureus* by subtracting the initial image of gold nanostars. We measured the RGB values from each well and determined the maximum change in each component. The red component of RGB model showed the maximum change in intensity. Thus, the red component was plotted against the CTAB and gold seed amounts (Fig. 3 b). This observation correlates closely with the light absorption peak and FWHM measured previously (Fig. 2 c,d). The green and blue components also change in a similar manner but the magnitude of change is smaller (Fig. S3). Fig. 3 b) suggests that more branched and larger nanostars show a greater color change in the presence of *S. aureus*. Interestingly, the general trend shown in Fig. 3 b) matched the trend throughout our findings in both absorbance peak and FWHM, suggesting a consistent theme that the size and degree of branching of nanostars significantly impact optical properties and govern detection performance in a similar manner. We also studied the evolution of color change over time for each of the nanostars. Initial onset of color change was immediate and visually discernible in less than 5 minutes for most samples. This is seen in Fig. 3 c) as the contour plot shows a change of up to 60 units of intensity within 300 seconds in the red component for the most sensitive gold nanostars. We observed that the color changes saturated after about 40 minutes. The plot confirms that the highest seed volume nanostars with smallest sizes and least branching show negligible color change due to high colloidal stability, while the most rapid color change occurs in nanostars synthesized using lowest seed volumes with biggest sizes and highest branching. This is in part because branching increases effective surface area and spatial extent, allowing gold nanostars to aggregate around the bacteria and therefore produce a more substantial change in color. The ideal formulation of nanostars will be stable in saline and change drastically in the presence of *S. aureus*. We quantified this criterion by subtracting the two images in Fig. 3 a) and determining the RGB values of the subtracted image. Since the red component demonstrates maximum change, the well with the highest difference in red provides the best formulation for application in pathogen detection. We observed that the nanostar solution synthesized using 125 mg CTAB and 240 μL gold nanoseed precursor was the optimal formulation. These nanostars have a small enough size to be stable in high salt concentrations and yet are branched enough to aggregate around *S. aureus* and cause a drastic color change. This optimal formulation of gold nanostars was used to test the effect of excess CTAB concentration on the detection of *S. aureus*. The results, seen in Fig. S4, demonstrate that there was negligible change between different concentrations of excess CTAB used. If the solution was devoid of CTAB (as in the Millipore water resuspension) after synthesis, gold nanostars would aggregate and change color in saline control as well. Thus, a small amount of CTAB is indeed necessary in solution after synthesis to prevent aggregation of the gold nanostars in saline (with ~0.006% broth).

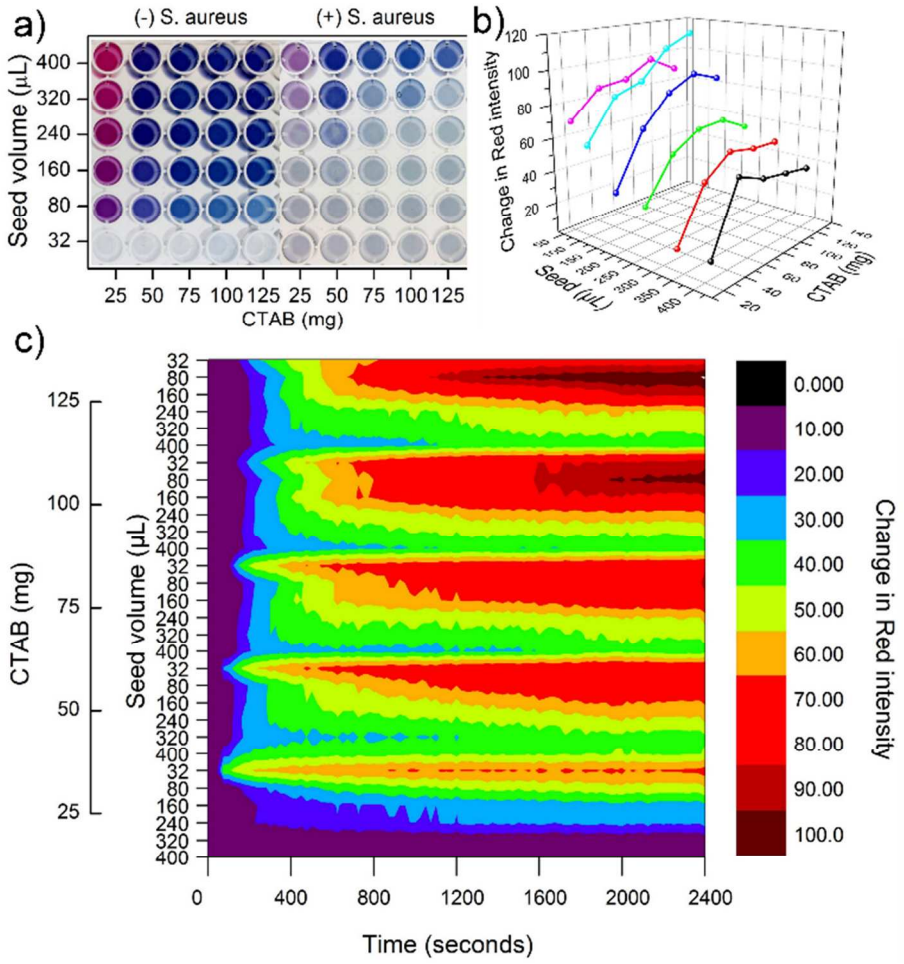

Fig. 3. Color change of gold nanostars in the presence of *Staphylococcus aureus*: a) Significant visible color change in the presence of $5x10^5$ CFU/well *S. aureus* in a 96-well microplate; b) the final, maximum color change in the red component of RGB color model plotted against the gold seed and CTAB amounts; c) Evolution of the change in intensity of red component of color over time for each sample.

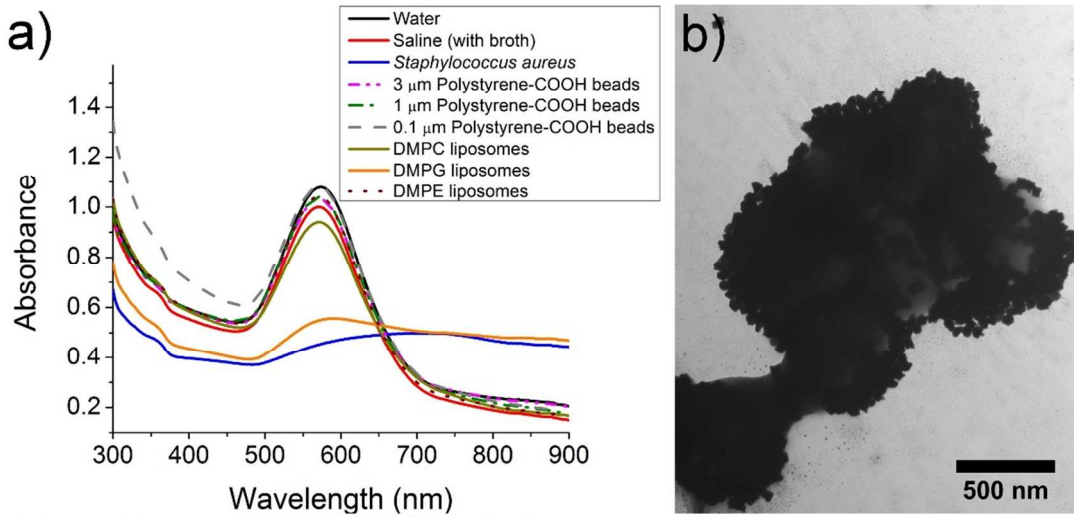

Fig. 4. Selectivity of the optimal formulation of gold nanostars: a) UV-Visible absorption spectra of gold nanostars in water, in saline with ~0.006% broth, in the presence of *S. aureus*, in the presence of 3 µm, 1 µm and 0.1 µm carboxylic acid functionalized polystyrene particles, in the presence of 1,2-dimyristoyl-sn-glycero-3-phosphocholine (DMPC) liposomes, 1,2-dimyristoyl-*sn*-glycero-3-phospho-(1'-rac-glycerol) (DMPG) liposomes and 1,2-dimyristoyl-*sn*-glycero-3-phosphoethanolamine (DMPE) liposomes; b) Transmission electron microscopy (TEM) image of gold nanostars aggregating around *S. aureus*.

RSC Advances RSCPublishing

COMMUNICATION

3.4. Selectivity of gold nanostars: UV-Visible absorption spectra

In order to better understand the cause of aggregation of CTAB-coated gold nanostars around *S. aureus,* we tested the interaction of gold nanostars with a variety of charged particles. Polystyrene microparticles functionalized with carboxylic acid were used to provide a negative surface charge, which has the potential to aggregate the positively charged CTAB-coated gold nanostars. Three different sizes of polystyrene microparticles were used to explore the effect of size on the aggregation of gold nanostars, where the 1 μm microparticles are most similar in size to *S. aureus*. We also used three different kinds of liposomes to explore the interaction between gold nanostars and charged phospholipids which could be responsible for the attraction between bacteria and gold nanostars. DMPC and DMPE terminate in a choline and ethanolamine group respectively and thus are zwitterionic. DMPG terminates in a glycerol group and hence the phosphate causes the liposomes to be overall negatively charged. Fig. 4 a) shows the UV-Vis spectra of the optimal formulation of gold nanostars (125 mg CTAB, 240 μL gold seed) in the presence of water, saline, *S. aureus,* polystyrene microparticles and phospholipids. The spectra in Fig. 4 a) demonstrate minimal change in saline, polystyrene microparticles and DMPC and DMPE liposomes, while highlighting a drastic broadening and flattening of the peak in *S. aureus* and DMPG liposome solutions which confirms the shift in plasmon resonance of the gold nanostars. These spectra are consistent with the observed color change in the microplates from solid blue to a translucent grey in the presence of *S. aureus*. We confirmed that the color change of gold nanostars was due to near complete aggregation around the *S. aureus* (Fig. 4 b) by imaging the samples using TEM. This aggregation is caused by electrostatic interactions between the CTAB-coated gold nanoparticle surface that is positively charged (zeta potential of +38.0 mV) and the cell wall of *S. aureus* that is negatively charged (zeta potential of -24.2 mV). Our results are in agreement with the work of Berry *et al.*[28] where they explained that the mechanism of aggregation of CTAB-coated gold nanorods around gram-positive *Bacillus cereus* is the strong electrostatic interactions between positively charged CTAB molecules and negatively charged teichoic acids on the surface of bacteria.[28] Teichoic acid is expressed on the surface of gram-positive bacteria and it includes several phosphate groups, which provide a polyanionic surface with a high density of negative surface charge. As demonstrated by Fig. 4 a), a polyanionic surface is necessary for the aggregation of CTAB-coated gold nanostars since only negatively charged DMPG liposomes led to substantial aggregation. On the other hand, polystyrene particles with monoanionc carboxylic acid and zwitterionic liposomes had insufficient negative charge to cause a significant color change. Since only DMPG liposomes cause a color change comparable to bacteria, the aggregation of gold nanostars requires interaction with several negatively charged groups. Thus, the aggregation and color change of CTAB-coated gold nansotars is selective to bacteria and polyanionic particles in comparison to other particles with only monoanionic or zwitterionic charges. This work avoids the use of antibodies and aptamers and only exploits electrostatic interactions for colorimetric detection. Thus, there are some limits to specificity but since the distribution of charges is expected to be different in different strains of bacteria, these interactions can potentially be exploited for differentiating between bacteria in the future.

4. Conclusion

We demonstrated that the size and degree of branching of gold nanostars can be controlled by varying the amount of gold nanoseed precursor and CTAB added to the formulation. We used CTAB-coated gold nanostars for rapid (<5 min) instrument-free colorimetric detection of *S. aureus* at its infective dose without the use of any targeting ligands such as antibodies or aptamers. The size and branching of gold nanostars control the rate and degree of color change in the presence of *S. aureus*. An optimal formulation of gold nanostars (125 mg CTAB and 240 μL gold nanoseed precursor) provides maximum contrast in color between *S. aureus* and saline (with ~0.006% broth) and also a selective response in comparison to polystyrene microparticles and liposomes. TEM confirmed that the mechanism of color change was indeed the aggregation of gold nanostars around the bacteria caused by electrostatic interactions. Thus, CTAB-coated gold nanostars are a promising platform for rapid colorimetric detection of pathogens at the relevant infective dose.

Acknowledgements

The authors would like to thank Mohammadreza Khorasaninejad and Professor Simarjeet Saini for their advice on image processing, Dr. David McCanna for his help with microbial culture, and Professor. Pu Chen for providing his Zetasizer. This work was financially supported by the Natural Sciences and Engineering Research Council of Canada (NSERC) and 20/20 NSERC – Ophthalmic Materials Network. M. S. Verma is grateful for the NSERC Vanier Canada Graduate Scholarship. P. Z. Chen is thankful for the NSERC Undergraduate Student Research Award.

Notes

[a] Department of Chemical Engineering, University of Waterloo, 200 University Avenue W, Waterloo, Ontario, Canada, N2L 3G1
[b] Waterloo Institute for Nanotechnology, University of Waterloo, 200 University Avenue W, Waterloo, Ontario, Canada, N2L 3G1
[c] Center for Contact Lens Research, University of Waterloo, 200 University Avenue W, Waterloo, Ontario, Canada, N2L 3G1
[+] Authors contributed equally
*Corresponding author. Tel. +1 519-888-4567 x 38605; Fax: +1 519-888-4347; E-mail: frank.gu@uwaterloo.ca

Electronic Supplementary Information (ESI) available: Figures showing the minor diameter, distribution of nanostar branches, maximum color change and effect of CTAB on color change are included in supplementary information. Supplementary video showing color change is also available.

References

1 T. Vo-Dinh, A. M. Fales, G. D. Griffin, C. G. Khoury, Y. Liu, H. Ngo, S. J. Norton, J. K. Register, H. N. Wang and H. Yuan, *Nanoscale,* 2013, **5,** 10127-10140.
2 S. K. Dondapati, T. K. Sau, C. Hrelescu, T. A. Klar, F. D. Stefani and J. Feldmann, *ACS Nano,* 2010, **4,** 6318-6322.
3 He Sha, Liu DingBin, Wang Zhuo, Cai KaiYong and Jiang XingYu, *Sci China Phys Mech Astron,* 2011, **54,** 1757-1765.
4 S. A. Khan, A. K. Singh, D. Senapati, Z. Fan and P. C. Ray, *Chem.Commun.(Camb),* 2011, **47,** 9444-9446.
5 C. G. Khoury, T. Vo-Dinh, *J.Phys.Chem.C,* 2008, **112,** 18849-18859.
6 H. Yuan, A. M. Fales, C. G. Khoury, J. Liu and T. Vo-Dinh, *J.Raman Spectrosc.,* 2013, **44,** 234-239.
7 L. Vigderman, E. R. Zubarev, *Langmuir,* 2012, **28,** 9034-9040.
8 L. Rodriguez-Lorenzo, R. A. Alvarez-Puebla, F. Javier Garcia de Abajo and L. M. Liz-Marzan, *J.Phys.Chem.C,* 2010, **114,** 7336-7340.
9 V. Giannini, R. Rodriguez-Oliveros and J. A. Sanchez-Gil, *Plasmonics,* 2010, **5,** 99-104.
10 E. N. Esenturk, A. R. H. Walker, *J.Raman Spectrosc.,* 2009, **40,** 86-91.
11 P. Senthil Kumar, I. Pastoriza-Santos, B. Rodriguez-Gonzalez, F. Javier Garcia de Abajo and L. M. Liz-Marzan, *Nanotechnology,* 2008, **19,** 015606-4484/19/01/015606. Epub 2007 Nov 29.
12 H. Yuan, C. G. Khoury, H. Hwang, C. M. Wilson, G. A. Grant and T. Vo-Dinh, *Nanotechnology,* 2012, **23,** 075102-4484/23/7/075102. Epub 2012 Jan 20.
13 W. Lu, A. K. Singh, S. A. Khan, D. Senapati, H. Yu and P. C. Ray, *J.Am.Chem.Soc.,* 2010, **132,** 18103-18114.
14 D. Kozanoglu, D. H. Apaydin, A. Cirpan and E. N. Esenturk, *Org.Electron.,* 2013, **14,** 1720-1727.
15 L. Shao, A. S. Susha, L. S. Cheung, T. K. Sau, A. L. Rogach and J. Wang, *Langmuir,* 2012, **28,** 8979-8984.
16 T. K. Sau, A. L. Rogach, M. Doblinger and J. Feldmann, *Small,* 2011, **7,** 2188-2194.
17 S. Trigari, A. Rindi, G. Margheri, S. Sottini, G. Dellepiane and E. Giorgetti, *J.Mater.Chem.,* 2011, **21,** 6531-6540.
18 S. Barbosa, A. Agrawal, L. Rodriguez-Lorenzo, I. Pastoriza-Santos, R. A. Alvarez-Puebla, A. Kornowski, H. Weller and L. M. Liz-Marzan, *Langmuir,* 2010, **26,** 14943-14950.
19 K. El-Boubbou, C. Gruden and X. Huang, *J.Am.Chem.Soc.,* 2007, **129,** 13392-13393.
20 L. Chen, F. S. Razavi, A. Mumin, X. Guo, T. Sham and J. Zhang, *RSC Adv.,* 2013, **3,** 2390-2397.
21 P. Laurino, R. Kikkeri, N. Azzouz and P. H. Seeberger, *Nano Lett.,* 2011, **11,** 73-78.
22 V. Velusamy, K. Arshak, O. Korostynska, K. Oliwa and C. Adley, *Biotechnol.Adv.,* 2010, **28,** 232-254.
23 M. D. Adhikari, B. R. Panda, U. Vudumula, A. Chattopadhyay and A. Ramesh, *RSC Adv.,* 2012, **2,** 1782-1793.
24 Y. Wang, Z. Ye and Y. Ying, *Sensors (Basel),* 2012, **12,** 3449-3471.
25 N. Karoonuthaisiri, R. Charlermroj, U. Uawisetwathana, P. Luxananil, K. Kirtikara and O. Gajanandana, *Biosens.Bioelectron.,* 2009, **24,** 1641-1648.
26 P. Schmid-Hempel, S. A. Frank, *PLoS Pathog.,* 2007, **3,** 1372-1373.
27 Y. C. Chang, C. Y. Yang, R. L. Sun, Y. F. Cheng, W. C. Kao and P. C. Yang, *Sci.Rep.,* 2013, **3,** 1863.
28 V. Berry, A. Gole, S. Kundu, C. J. Murphy and R. F. Saraf, *J.Am.Chem.Soc.,* 2005, **127,** 17600-17601.
29 S. C. Hayden, G. Zhao, K. Saha, R. L. Phillips, X. Li, O. R. Miranda, V. M. Rotello, M. A. El-Sayed, I. Schmidt-Krey and U. H. Bunz, *J.Am.Chem.Soc.,* 2012, **134,** 6920-6923.
30 H. M. Chen, H. C. Peng, R. S. Liu, K. Asakura, C. L. Lee, J. F. Lee and S. F. Hu, *J Phys Chem B,* 2005, **109,** 19553-19555.
31 M. Grzelczak, J. Perez-Juste, P. Mulvaney and L. M. Liz-Marzan, *Chem.Soc.Rev.,* 2008, **37,** 1783-1791.
32 C. L. Nehl, H. Liao and J. H. Hafner, *Nano Lett.,* 2006, **6,** 683-688.
33 T. K. Sau, A. L. Rogach, *Adv Mater,* 2010, **22,** 1781-1804.
34 H. Wu, C. Chen and M. H. Huang, *Chem. Mater.,* 2009, **21,** 110-114.
35 H. Min-Chen, R. Liu and D. P. Tsai, *Cryst. Growth Des.,* 2009, **9,** 2079-2087.
36 F. Xia, X. Zuo, R. Yang, Y. Xiao, D. Kang, A. Vallee-Belisle, X. Gong, J. D. Yuen, B. B. Hsu, A. J. Heeger and K. W. Plaxco, *Proc.Natl.Acad.Sci.U.S.A.,* 2010, **107,** 10837-10841.
37 S. Link, M. A. El-Sayed, *Int. Rev. Phys. Chem.,* 2000, **19,** 409-453.
38 F. Hao, C. L. Nehl, J. H. Hafner and P. Nordlander, *Nano Lett.,* 2007, **7,** 729-732.